Remote Sensing of Environment 295 (2023) 113648

Contents lists available at ScienceDirect

Remote Sensing of Environment

journal homepage: www.elsevier.com/locate/rse

Evaluating MODIS snow products using an extensive wildlife camera network

Catherine Breen [a,*], Carrie Vuyovich [b], John Odden [c], Dorothy Hall [d], Laura Prugh [a]

[a] Department of Environmental and Forest Sciences, University of Washington, Seattle, WA, USA
[b] Hydrological Sciences Laboratory, NASA Goddard Space Flight Center, Greenbelt, MD, USA
[c] Norwegian Institute for Nature Research, Post Office Box 5685 Torgarden, Trondheim, Norway
[d] Earth System Science Interdisciplinary Center, University of Maryland College Park, College Park, MD, USA.

ARTICLE INFO

Edited by Dr. Menghua Wang

Keywords:
Validation
Norway
Remote cameras
Gap-filling
MODIS
Snow

ABSTRACT

Snow covers a maximum of 47 million km^2 of Earth's northern hemisphere each winter and is an important component of the planet's energy balance, hydrology cycles, and ecosystems. Monitoring regional and global snow cover has increased in urgency in recent years due to warming temperatures and declines in snow cover extent. Optical satellite instruments provide large-scale observations of snow cover, but cloud cover and dense forest canopy can reduce accuracy in mapping snow cover. Remote camera networks deployed for wildlife monitoring operate below cloud cover and in forests, representing a virtually untapped source of snow cover observations to supplement satellite observations. Using images from 1181 wildlife cameras deployed by the Norwegian Institute for Nature Research (NINA), we compared snow cover extracted from camera images to Moderate Resolution Imaging Spectroradiometer (MODIS) snow cover products during winter months of 2018–2020. Ordinal snow classifications (scale = 0–4) from cameras were closely related to normalized difference snow index (NDSI) values from the MODIS Terra Snow Cover Daily L3 Global 500 m (MOD10A1) Collection 6 product (R^2 = 0.70). Tree canopy cover, the normalized difference vegetation index (NDVI), and image color mode influenced agreement between camera images and MOD10A1 NDSI values. For MOD10A1F, MOD10A1's corresponding cloud-gap filled product, agreement with cloud-gap filled values decreased from 78.5% to 56.4% in the first three days of cloudy periods and stabilized thereafter. Using our camera data as validation, we derived a threshold to create daily binary maps of snow cover from the MOD10A1 product. The threshold corresponding to snow presence was an NDSI value of 40.50, which closely matched a previously defined global binary threshold of 40 using the MOD10A2 8-day product. These analyses demonstrate the utility of camera trap networks for validation of snow cover products from satellite remote sensing, as well as their potential to identify sources of inaccuracy.

1. Introduction

Seasonal snow covers 31% of the Earth's land surface each year, playing an integral role in habitat quality for wildlife, water storage for hydrological processes, and human uses such as agriculture, forestry, and tourism (Mankin et al., 2015; Rizzi et al., 2018). Warming temperatures have reduced snow cover extent globally, but these changes vary strongly among regions (Brown and Mote, 2009; Solomon et al., 2007). Accurate snow cover mapping within and across years is thus needed to inform regional forecasting and climate change mitigation efforts.

Snow cover is typically measured using ground observations, modeling, and remote sensing at scales that range from point measurements (e.g., ground observations) to kilometers (e.g., passive microwave sensors at 25-km resolution). Remote sensing from satellites is a powerful tool because satellites provide information across broad spatial coverages and at fine temporal scales, enabling global and regional snow cover maps where in situ measurements may not be possible (Nolin, 2010). NASA's Moderate Resolution Imaging Spectroradiometer (MODIS) Collection 6 product provides a daily or every other day 500-m resolution optical image from which snow maps are derived. Daily MODIS snow observations are highly suitable for continuous snow monitoring, which is desirable for many applications, including wildlife science (Boelman et al., 2019). For example, daily MODIS snow maps

* Corresponding author at: Department of Environmental and Forest Sciences, University of Washington, Seattle, WA 98195, USA.
E-mail address: cbreen@uw.edu (C. Breen).

https://doi.org/10.1016/j.rse.2023.113648
Received 5 December 2022; Received in revised form 18 May 2023; Accepted 23 May 2023
Available online 13 June 2023

have been used to successfully detect changes in bird nesting success and shifts in the timing of mammal migrations (Laforge et al., 2021; Madsen et al., 2007).

The most recent version of the MODIS products (Collection 6.1) includes a daily 500-m global snow product, MOD10A1, and a daily cloud-gap filled (CGF) 500-m global snow product, MOD10A1F. Both are suitable for use as inputs in hydrological, ecological, and climate models (Bokhorst, 2016; Dong and Menzel, 2016). MOD10A1 and MOD10A1F provide normalized difference snow index (NDSI) values based on the high reflectance of snow in the visible band and low reflectance in the near-infrared band, ranging from 0 (snow-free) to 100 (completely snow-covered). NDSI values lower than 100 can be completely snow-covered (Klein et al., 1998), but adjusting NDSI values to a fractional snow cover is no longer included in MODIS products as it is region-dependent and other factors may affect when MODIS underestimates snow. The overall accuracy of the MOD10A1 product is estimated to fall between 79.5 and 96% depending on the tree cover density, snow depth, and solar zenith angle in the region of interest (Coll and Li, 2018; Franklin, 2020; Hall et al., 2019a; Hall and Riggs, 2007). Optical sensors are obstructed by tree cover, and shallow snow might not be bright enough to reflect solar radiation since the underlying material is likely to be darker (Liang et al., 2008). At high solar zenith angles, chances are higher that sensors will be obstructed by clouds and experience higher atmospheric distortion (Xin et al., 2012), both of which can also obscure or scatter light, decreasing the accuracy of observations.

Cloud masking in MOD10A1 greatly reduces coverage (Hall et al., 2019a), and MOD10A1F improves coverage by filling all cloud-masked pixels. Each cloud-masked pixel is given the most recently observed snow cover value, along with a corresponding "cloud persistence" value for the age in days of the snow observation. This product has been used in applications such as hydrological snow trend studies (Hao et al., 2022) and analyses of snow cover impacts on wildlife (Mahoney et al., 2018). The cloud-gap filled product has been shown to return similar accuracy as MOD10A1 in the western US where cloudy periods are typically brief (Hall et al., 2019a), whereas accuracy is lower in the northeastern and northwestern US where longer cloudy periods are common (Gao et al., 2011; Hall et al., 2010). Beyond the US, validation of the MOD10A1F product is sparse due to the recency of the product availability. Weather stations and other sensors improved MOD10A1F maps in China (Hao et al., 2022), but more work in diverse areas with longer cloudy episodes, such as high latitude regions, is needed to understand the accuracy of the MOD10A1F product in those areas. Understanding accuracy may inform a region-dependent threshold after which additional cloudy days may result in unreliable snow cover estimates, and indicate when alternative sources for snow cover, such as weather stations or other ground observations, should be used instead of gap-filled values.

Binary products can be developed from the current MODIS snow-cover products and may be used to map snow presence/absence. Early MODIS snow-cover products categorized pixels as "snow" if the NDSI was >40, using Landsat fractional snow-covered area maps from Prince Albert National Park in Saskatchewan, Canada (Klein et al., 1998). Later, a binary map developed from MOD10A2 categorized a pixel as "snow" if any pixel within an 8-day period had an NDSI value >10 (Hall et al., 2002). The lower threshold increased snow detection but at the cost of increased false positives. Now, the threshold for snow presence is considered region dependent (Thapa et al., 2019; Zhang et al., 2019), and the end-user is recommended to determine the threshold above which the corresponding pixel should be identified as snow covered (Riggs et al., 2017). Given the utility of binary snow products for monitoring snow phenology and subsequent applicability to wildlife studies (Curk et al., 2020; Madsen et al., 2007; Thapa et al., 2019), more work is needed to develop daily binary snow maps for specific regions.

In this study, we use cameras deployed in remote locations for wildlife monitoring, often referred to as "camera traps," to evaluate the MODIS/Terra MOD10A1 and MOD10A1F products and derive a regional threshold for daily binary snow-covered maps in Scandinavia. Wildlife camera trap networks have underutilized potential for satellite validation that could be a valuable supplement to traditional validation methods based on other satellites (Crawford, 2015; Huang et al., 2011), weather stations, and ground collection (Negi et al., 2007). Cameras provide environmental monitoring (Brown et al., 2016; Sonnentag et al., 2012), with visual information about environmental conditions along with a timestamp. While single cameras have a limited field of view, they can be set up in networks of up to many hundreds of cameras across large regions (Forrester et al., 2016; Garvelmann et al., 2013). Databases are increasingly available to archive camera images across networks, furthering the potential for global camera networks to improve environmental monitoring (Steenweg et al., 2017). For example, Wildlife Insights currently hosts over 35 million images from 20,000 camera deployments worldwide (https://www.wildlifeinsights.org/home). Cameras operate below cloud cover and tree canopy, and they are particularly advantageous for monitoring snow cover because they can operate for months or years in sub-freezing conditions and difficult-to-reach locations (Tobler et al., 2015).

Wildlife camera traps have been used successfully to evaluate satellite measures of greenness (Sun et al., 2021) and to provide information on snowpack dynamics at localized spatial scales (Hofmeester et al., 2019; Sirén et al., 2018). Hofmeester et al. (2019) visually categorized snow cover from camera trap images to assess changes in spring and autumn molting of mountain hare (*Lepus timidus*). Sirén et al. (2018) found strong correlations between depth readings on snow poles and data from the Snow Data Assimilation System (SNODAS) at 80 cameras in Vermont. However, extracting information from camera images can be challenging. Camera traps use an infrared flash in low light settings, resulting in grey-scale images that can make differentiating among objects more difficult (Beery et al., 2019). Camera traps therefore have great potential but require more work investigating their utility as ground-based remote sensing networks for monitoring snow at broader scales.

Using three years of camera trap images from a network of 1181 cameras in Norway and Sweden managed by the Norwegian Institute for Nature Research (NINA), we compared snow data extracted from camera images to MOD10A1 and MOD10A1F NDSI snow cover products. We quantified agreement between snow cover values from cameras and MODIS NDSI, examining factors we hypothesized a priori would affect agreement. We predicted the following:

1. Agreement would be higher between cameras and NDSI at extreme values for snow cover, whereas agreement would be lower when the snow is patchy (i.e., moderate NDSI values) due to differences in scales between MODIS pixels (500 m) and camera fields of view (~20–80 m).
2. Factors that have been shown to affect MODIS accuracy will affect camera and MODIS agreement, such that agreement will be lower when canopy cover and latitude are higher (Xiao et al., 2022; Xin et al., 2012).
3. Factors that have been shown to affect image quality will affect camera and MODIS agreement, such that images with low lighting taken in grey-scale (i.e., with infrared flash) will have lower agreement with NDSI than images taken in full color.
4. Camera observations should agree more with MODIS observations on clear sky days compared to cloudy days, and cloud persistence should decrease the agreement between cameras and the cloud gap filled NDSI product.

We derived a binary MOD10A1 product of snow cover, using camera data to identify a NDSI threshold corresponding to snow presence.

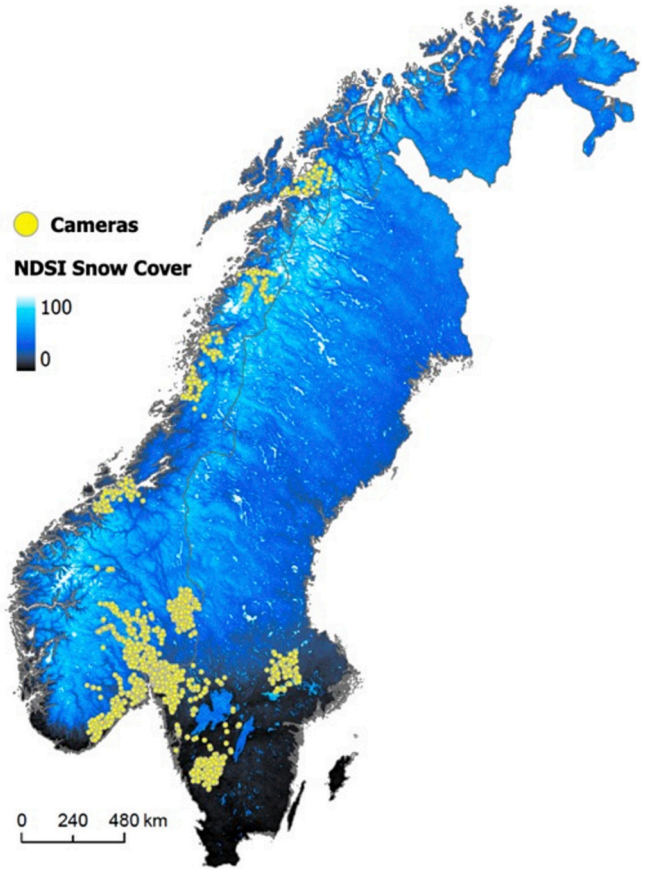

Fig. 1. Locations of Scandcam cameras (yellow points, $n = 1181$) in Norway and Sweden shown over a composite snow cover map created from MOD10A1 Version 6 that shows mean NDSI snow cover values across the three winters of this study (January – March 2018, October 2018 – April 2019, October 2019 – April 2020). (For interpretation of the references to color in this figure legend, the reader is referred to the web version of this article.)

2. Methods

2.1. Study area

We used images from camera traps in the Scandcam network. Scandcam is a long-term, year-round study established in 2010 by the Norwegian Institute for Nature Research to monitor recovering Eurasian lynx (*Lynx lynx*). Our dataset includes images from three winter seasons: 1) January 1 – March 2018, 2) October 1, 2018 – March 2019, and 3) October 2019 – March 2020.

Scandcam camera trap locations are optimized for lynx detection across Norway and southern Sweden (59° – 69° N, 8° – 16° E), with no more than one camera per 2 km^2 area across a 350,000 km^2 area (Fig. 1; Carricondo-Sanchez et al., 2017). Cameras span a 10° latitudinal gradient, with deeper snow generally occurring in the north and inland than along the coast (Saloranta, 2012). Snow usually arrives in Norway and Sweden in early October at high elevations and northern areas and melts by early April, although sites farther north can remain snow-covered into summer (Saloranta, 2012). Because the cameras were deployed to detect lynx, they were placed in lynx habitat such as forests and sub-alpine areas, but they varied in whether they were under closed-canopy or open-canopy areas. Southern Norway and Sweden are characterized by boreal coniferous forest dominated by Norway spruce (*Picea abies*) and Scots pine (*Pinus sylvestris*). In the north, forest composition transitions to alpine vegetation dominated by birch species (*Betula pendula* and *Betula pubescens)* (Bouyer et al., 2015).

2.2. Data

2.2.1. MODIS data

NDSI values were extracted at all camera locations ($n = 1181$) for all days in the study period from the MOD10A1 product on the Google Earth Engine public data archive ($n = 770$ days; Hall et al., 2016). To quantify the percentage of usable MOD10A1 NDSI values during our study period, we divided the number of non-null NDSI values by the total number of values (including cloud-masked pixels with "NA" values). The MOD10A1F product was downloaded as GeoTiffs for the same days from the EarthData platform (https://search.earthdata.nasa.gov/) and uploaded to Google Earth Engine (GEE). MOD10A1F NDSI

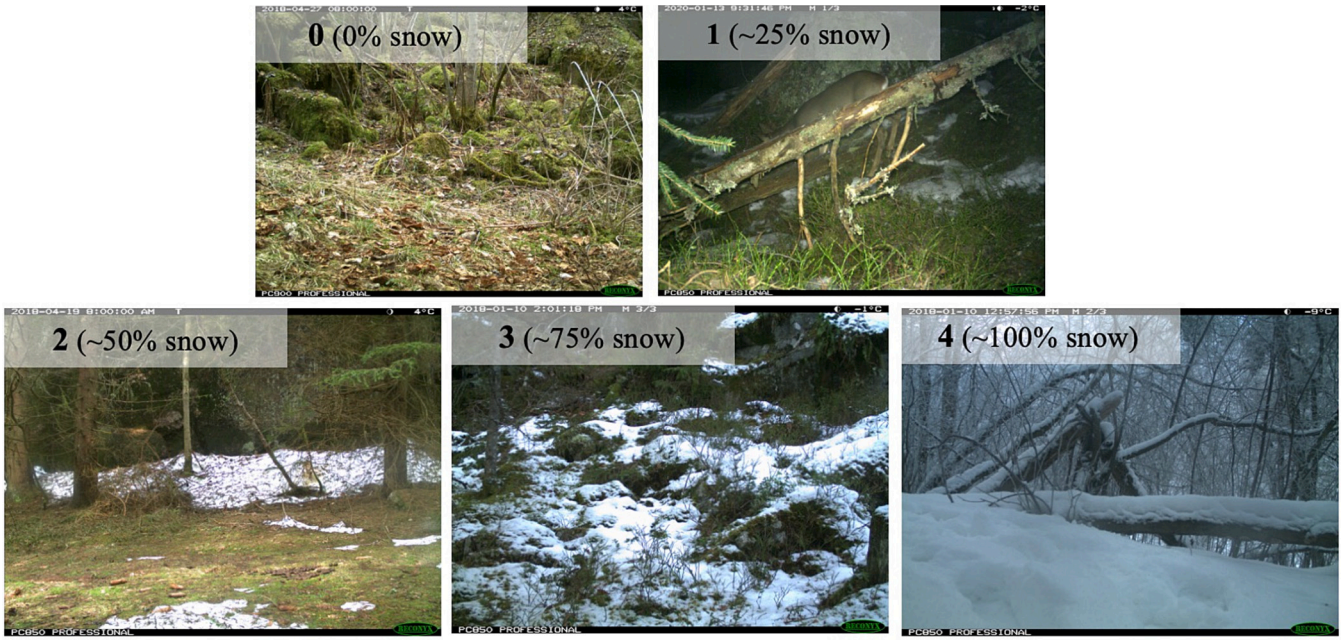

Fig. 2. Example remote camera images for snow classification. Snow cover was classified using an ordinal scale from 0 to 4, where 0 = 0% snow cover, 1 = ~25%, 2 = ~50%, 3 = ~75%, and 4 = ~100%.

and corresponding cloud persistence values were extracted for all cameras for the same days after ensuring both MODIS products matched projections (Appendix A1). Since MOD10A1F is not offered in the GEE archive, MOD10A1F was uploaded as individual tiles. In total, we processed 3392 tiles for the MOD10A1F product. We used the GEE Collection 6 MOD10A1 product rather than Collection 6.1 from EarthData, because Collection 6 is commonly used in other studies, and GEE has limits on the number of original assets one can store on the server. We used Collection 6.1 for MOD10A1F (cloud-gap filled) NDSI and cloud persistence products to make use of the most up-to-date version. Previous work has demonstrated that Collection 6.1 and Collection 6 have 99% correspondence, with revisions considered minor (Riggs et al., 2019).

2.2.2. Camera images

Cameras with either infrared flash or white flash (Reconyx model HC500, HC600, PC800, or PC900) were secured to trees approximately 1 m above the ground. Cameras were programmed to take a daily "timelapse" image at 8 AM or 12 AM, as well as anytime the camera was triggered by motion (e.g., from an animal walking by). For all cameras, for every day in our study years that there was a corresponding non-null MOD10A1 value, we selected one image per day from the Scandcam image inventory. The vast majority of photos were taken under low-light conditions resulting in a grey-scale image. To achieve a more balanced dataset to evaluate the effect of image color mode on snow labeling accuracy, we manually inspected all of the images to select a color image if available. We deferred to the timelapse image when taken in white flash or daylight hours, or a daytime motion-triggered image, when available. Images from the prior day or the day after the image of interest were also inspected and labeled if it was hard to discern snow due to lighting conditions.

To assess the effects of cloud cover, we labeled a subset of images that corresponded to 250 random days from the MOD10A1F product (100 days for each of the full winter seasons, and 50 days for the partial season). Additionally, we included images that were inspected while labeling MOD10A1 images (n = 510 images). These included both before and after images corresponding to MOD10A1 values to help confirm the amount of snow. While there is potentially a bias that these images would favor lower cloud persistence values, we examined a histogram and found a similar distribution of cloud persistence values compared to the distribution of cloud persistence values from the full MOD10A1F dataset (Appendix A2).

Images were labeled using Timelapse (http://saul.cpsc.ucalgary.ca/time-lapse/), a freely available camera trap labeling software for wildlife ecologists. The software automatically extracts metadata including time and date, and it provides a customizable interface that observers use to label photos. All data can then be exported as a .csv file. Snow cover was manually labeled using the software's user interface on an ordinal scale that ranged from 0 (no snow) to 4 (full snow coverage). These categories matched those used for snow cover classification at Norwegian weather stations (Lussana et al., 2018): 0 corresponded to 0% snow cover, 1 to ~25% snow cover, 2 to ~50%, 3 to ~75%, and 4 to ~100% (Fig. 2). Images were initially labeled by two people, but testing of a double-labeled subset revealed low agreement among observers (kappa coefficient κ = 0.45; McHugh, 2012). There was complete agreement at label 0, moderate agreement for values 1–3 (κ = 0.51) and low agreement for label 4 (κ = 0.10). The low agreement at label 4 was a result of the less-experienced labeler incorrectly labelling low-light images with snow as "no snow." Thus, the more-experienced observer (C. B.) labeled all images.

2.3. Assessing agreement between camera images and MODIS snow values

To evaluate the relationship between image labels and MOD10A1 (H1), we fit a general linear model using the ordinal image labels as a continuous predictor variable and MOD10A1 NDSI as the response variable. Since NDSI values have been noted to "plateau" at higher snow values depending on the normalized difference vegetation index (NDVI) at that pixel (Klein et al., 1998), a polynomial term was included to account for potential non-linearity. All models were fit using program R (version 4.2.1).

Table 1
Covariates used to analyze agreement between MODIS and image-labeled snow values. Range of each factor is provided. MODIS cloud persistence values were only used to assess MOD10A1F (i.e., the cloud-gap filled product) agreement with camera images.

Covariate	Range	Resolution	Hypothesized effect on agreement
Daily MODIS NDVI	−1.0–1.0	500 m	Increasing vegetation will prevent MODIS obs., decreasing agreement with ground obs.
Landsat tree canopy cover	0–100%	30 m	Increasing tree canopy cover will prevent MODIS obs., decreasing agreement with ground obs.
Image color mode	Color (1) or Grey-scale (0)	20–30 m[1]	The infrared red flash will decrease the saturation of the image (converting it to grey-scale), increasing the difficulty of differentiating snow from other aspects of the landscape.
Latitude	59.0–69.0	1 degree	Increasing latitude increases angle of MODIS obs., increasing angular distortion and decreasing agreement with ground obs.
MODIS Cloud Persistence	0–40 days	500 m	Increasing cloud cover days increases possibility of missed accumulation or melt events, decreasing agreement with ground obs.

[1] Resolution derived from the approximate range that wildlife cameras detect (Urbanek et al., 2019).

To test our prediction that agreement between MODIS and images would be highest at extreme values (H1), we compared agreement between MODIS NDSI snow cover values and snow cover from labeled camera images (hereafter called "image labels") across the ordinal image labels. We calculated agreement as:

$$Agreement = 100 - |MODIS - Camera| \quad (1)$$

Where *MODIS* is the NDSI value and *Camera* is the labeled image value after converting ordinal labels (0–4) to their corresponding percent cover values (0, 25, 50, 75, and 100). Agreement could range from 0 (i.e., complete disagreement) to 100 (i.e., complete agreement). Some amount of disagreement was expected from comparing ordinal image labels to continuous NDSI values. Thus, we caution that agreement levels should not be compared directly to R^2 values from traditional validations. Other studies that assessed MODIS NDSI accuracy using cameras and other ground sources converted NDSI values to binary snow and no snow values using a threshold and confusion matrix (Thapa et al., 2019; Zhang et al., 2019). We made use of the full range of NDSI values by not thresholding the values for agreement assessment, in order to statistically assess covariates that affected the level of agreement. We equate NDSI to a scale of 0–100% snow cover to represent the relationship between NDSI and snow cover in the absence of factors that may affect satellite accuracy. Taking the absolute value of agreement allowed for clearer interpretation of how different covariates affected the magnitude of disagreement regardless of its direction (see 2.4). We expected agreement to be highest at the extremes (i.e., labels ~0% and ~ 100%) and lowest for intermediate labels (i.e., labels ~25%, 50%, and 75%), so we fit a linear model with a polynomial term to allow for a parabolic shape.

Fig. 3. A grey-scale and color image from the camera on 22 November 2018 illustrates how light saturation affects the ability of an observer to identify snow cover. The image on left was the daily timelapse photo taken at 08:00 h during low light conditions, which triggered the camera to take the image in grey-scale (i.e., with infrared flash). The image on the right was triggered by a wolf (*Canis lupus*) passing by at 14:03 h, when there was enough light for a color image. The amount of snow in the color image is much easier to see.

2.4. Assessing agreement between MODIS snow products and factors influencing agreement

To identify factors affecting agreement between snow cover from image labels and the MOD10A1 product (H2 and H3), we used a general linear mixed-effects model to determine how tree canopy cover, latitude (a proxy for solar zenith), and image color mode affected the agreement between image labels and MOD10A1 NDSI values (Table 1; Eq. 2). We first tested covariates for correlation to avoid overfitting the model. We used Pearson's method for correlation between continuous variables and Kendall's method for correlation between continuous and our categorical variable (i.e., image color mode) and found that all correlations were below the commonly-used threshold of 0.7 (Dormann et al., 2013; Appendix A3). All correlations were also below the threshold for moderate correlations ($|r| = 0.4$), except for tree canopy cover and latitude, which was −0.404. To further examine multicollinearity among predictors, we implemented the variance inflation factor (VIF) test. All factors were below 1.2, lower than the conservative threshold of 3 (Zuur et al., 2010; Appendix A4). Temporal and spatial autocorrelation in snow datasets can inflate parameter estimates and type 1 error (Reinking et al., 2022). To evaluate spatial autocorrelation, we conducted Moran's I test using the *spdep* package in R (Bivand, 2022). We failed to detect spatial autocorrelation (Moran's I statistic = −0.007, $p = 0.55$), but we included Camera ID as a random effect to account for lack of independence among images taken from the same camera. To test for temporal autocorrelation, we followed the approach of Sirén et al. (2018) and created a relative date variable for each observation using the *timeDate* package in R (Wuertz et al., 2023). The package contains a function to convert a date to a relative number of days from a specified origin, defaulting to January 1, 1970. We tested for improved model fit using Akaike Information Criterion (AIC) values with and without including the relative date in an auto-regressive correlation structure (i.e., an "*ar1*" term) with camera station ID included as a grouping variable. Incorporating the *ar1* correlation structure had a lower AIC score [(ΔAIC = −1830.2 compared to the model without a correlation structure]. We therefore proceeded to use this structure for modeling agreement in Eq. (2). We included all covariates in a general linear mixed effects model with a Gaussian family using the *glmmTMB* package in R (Brooks et al., 2017):

$$Agreement \sim (1 \mid CameraID) + DailyNDVI + TreeCanopyCover + Latitude + ImageColorMode + ar1(RelativeDate + 0 \mid CameraID) \quad (2)$$

Agreement was calculated as described above in Eq. (1). Image color mode was classified as "Color" or "Grey-scale" by inspecting image saturation. Images taken with infrared flash have low light saturation and appear as black-and-white, grey-scale images (Fig. 3). After inspecting a histogram of saturation values from a subset of 60 images, there was a clear break between images in grey-scale and color at saturation values of 0.02 (Appendix A5). We then evaluated this threshold using a random subset of 1000 images and found 100% accuracy, so we labeled all images with values below 0.02 as grey-scale and above 0.02 as color.

Previous studies found that dense forests affected MODIS NDSI by causing an underestimation of the snow cover, using daily NDVI as a proxy for forest canopy (Hall and Riggs, 2007; Klein et al., 1998). MODIS NDVI is a vegetation index that provides information on vegetation canopy greenness, along with leaf area, and chlorophyll and canopy structure (Didan, 2015). NDVI in Norway varies spatially due to differences in vegetation from boreal, deciduous trees in southern Norway to alpine shrubs in northern Norway. Within a winter season, NDVI is highest in October and November and lowest in February and March, likely reflecting both deciduous trees losing canopy leaves in the fall, and seasonal snow covering ground vegetation in January to March (Appendix A6). To test the efficacy of NDVI as a proxy for tree canopy cover, we extracted the corresponding daily MODIS NDVI value at 500-m for each labeled image. We also extracted tree canopy cover from the 30-m Landsat Vegetation Continuous Fields tree cover layer, which estimates the percentage of horizontal ground covered by woody vegetation >5 m in height from 2015 (Townshend, 2016). Continuous predictor variables – tree canopy cover, latitude, and NDVI – were normalized by subtracting by the mean and dividing by the standard deviation. Model fit was evaluated by examining residuals for dispersion and outliers from the *DHARMa* package in R (Hartig, 2022; Appendix A9).

To test our prediction that agreement between MODIS and camera data would decline as the number of cloudy days (i.e., cloud persistence) increased (H4), we modeled the agreement between snow cover from image labels and the MOD10A1F product as a function of the cloud persistence value. Because we expected the relationship between agreement and the number of cloudy days to be non-linear, we ran a generalized additive mixed model with camera ID included as a random effect using the *mgcv* package in R (Eq. 3; Wood, 2017). We selected eight knots for the model, following recommendations for knots to be larger than the degrees of freedom (i.e., 6) plus 1 (Wood, 2017). Cloud persistence values equal to 0 (MOD10A1 values) were included to allow agreement comparison to clear sky days.

$$Agreement \sim (1 \mid Camera\ ID) + MOD10A1F\ Cloud\ Persistence \quad (3)$$

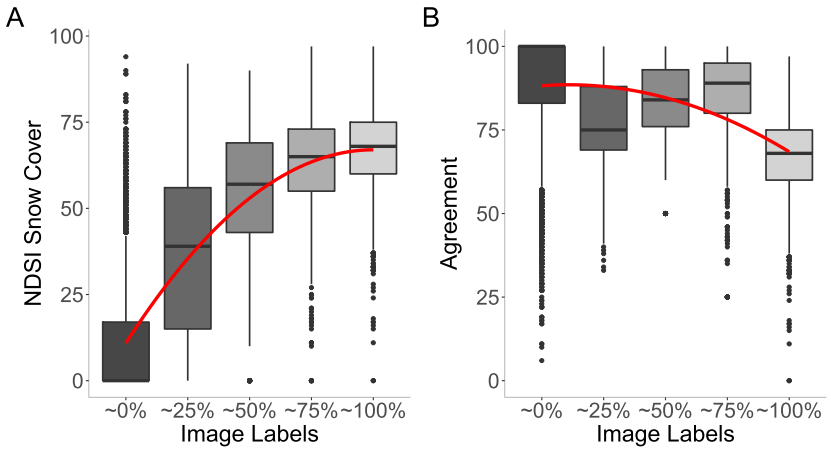

Fig. 4. A) Distribution of MOD10A1 NDSI values within each snow cover classification from labeled camera images, and B) agreement of snow cover values between MODIS and images within each snow cover classification. Images were labeled using an ordinal classification with 5 levels (0–4) corresponding to snow cover percentages shown. Agreement was defined as 100 minus the absolute difference between the image label and MOD10A1 NDSI snow value. Red lines show the best fit using linear models with polynomial terms. (For interpretation of the references to color in this figure legend, the reader is referred to the web version of this article.)

Table 2
Coefficient estimates, standard error (SE), t-values, and *p*-values from a general linear mixed model assessing factors that affect MODIS and camera agreement ($n = 8808$) for the three winter seasons: 1) January 1–March 2018, 2) October 1, 2018 – March 2019, and 3) October 2019 – March 2020. Continuous variables were normalized by subtracting the mean and dividing by the standard deviation prior to analysis. Image color mode is a categorical variable (1: color image; 0: grey-scale image). Camera identification was included as a random effect ($n = 658$). Model results without observations from October 2018 and October 2019 are included in Appendix A7. Results from the model without October data are similar, except that the effect size of NDVI changes from strongly positive to weakly negative.

Parameter	Estimate	SE	t-value	*p*-value
Intercept	78.88	0.40	196.37	<0.005
Latitude	−0.48	0.35	−1.37	0.17
NDVI	6.60	0.35	29.12	<0.005
Tree canopy cover	−0.93	0.32	−2.84	<0.005
Image color mode (color image)	1.73	0.47	3.63	<0.005

Agreement was calculated as described in 2.3 (Eq. 1). Data was sparse for persistence times > two weeks, (3% of data), so we limited analysis to 14 days.

2.5. Deriving a threshold for daily binary snow mapping in Norway

Image labels were converted from the 5-class ordinal scale to a binary classification by reclassifying all images labeled 1–4 as "snow" (with a corresponding 1 label), and all image labeled with a 0 as "no snow" (with a corresponding 0 label). We identified an optimal threshold for the MOD10A1 product by counting the number of true positives and false positives when converting to a binary product at each NDSI value. We plotted the true positive rate against the false positive rate at each threshold value to create a receiver-operating-characteristic (ROC) curve using the *pROC* package in R (Robin et al., 2011). The top left corner of the ROC curve is known as Youden's Index, or the maximum difference between the true positive and false positive rate (Youden, 1950). Because it weighs both true positive and false positive rates equally, it is considered the optimum threshold for a classifier when there is equal preference for both classes (Liu, 2012). In addition to generating a threshold for all cameras, we repeated this analysis separately for cameras within closed canopy (> 20% canopy cover; $n = 6229$ images) and open canopy (≤ 20% cover; $n = 2731$ images) because thresholds tend to be lower in areas of closed canopy cover (Chokmani et al., 2010).

3. Results

3.1. Labeled image and MODIS comparisons

Of the 1,703,702 MOD10A1 snow cover values obtained at all 1181 cameras during winters 2018–2020, 1,311,249 (76%) were null (cloud-masked). Daily labeled images corresponding to non-null values from MOD10A1 spanned 665 cameras ($n = 8918$ images). Cameras not included either had no corresponding non-null MODIS value or did not have images on file during our study period. There was a strong correlation between snow classification from the images and MOD10A1 NDSI values ($R^2 = 0.70$, NDSI $= -3.50*image^2 + 28.02*image + 10.90$, where *image* is the labeled value on the 0–4 scale), but the NDSI values from MODIS products plateaued at about 75 (Fig. 4A). We found overall strong agreement between snow cover from MODIS NDSI and camera images ($\bar{x} = 80.5\%$, 95% CI = 80.1–80.8; Fig. 4B). Consistent with H1, agreement was highest for images with label 0 (corresponding to ~0% snow cover; agreement $\bar{x} = 89.2\%$, 95% CI = 88.6–89.8). Contrary to H1, however, agreement was lowest for images with label 4 (corresponding to ~100% snow cover; agreement $\bar{x} = 67.1\%$, 95% CI = 66.7–67.5, Fig. 4B).

3.2. Factors that influence agreement between cameras and MODIS

As predicted by H3, latitude and tree canopy cover negatively affected agreement between snow cover derived from cameras and MOD10A1. However, only canopy cover had a statistically significant effect (Table 2). Although significant, the effect was relatively weak, and mapping the agreement at each camera relative to tree canopy cover showed that agreement was high in many areas with closed canopies (Fig. 5A-D). Contrary to expectations, NDVI was not strongly correlated with tree canopy cover ($r = 0.09$, Appendix A3) and had a significant positive effect on agreement: image labels and MODIS-derived snow cover were in better agreement in areas with higher daily NDVI. Average NDVI values in October were twice as high as any other month (Appendix A6), and October likewise had a relatively high proportion of 0 values with high agreement (Fig. 4B). Thus, we examined the effect of removing October observations from our model and found the effect of NDVI on agreement changed from strongly positive (coefficient value = 6.60) to weakly negative (coefficient = −0.075; Appendix A7). Our dataset was roughly split between color ($n = 4184$ images) and grey-scale ($n = 4733$ images), and image color mode positively affected agreement as predicted by H4 (Table 2).

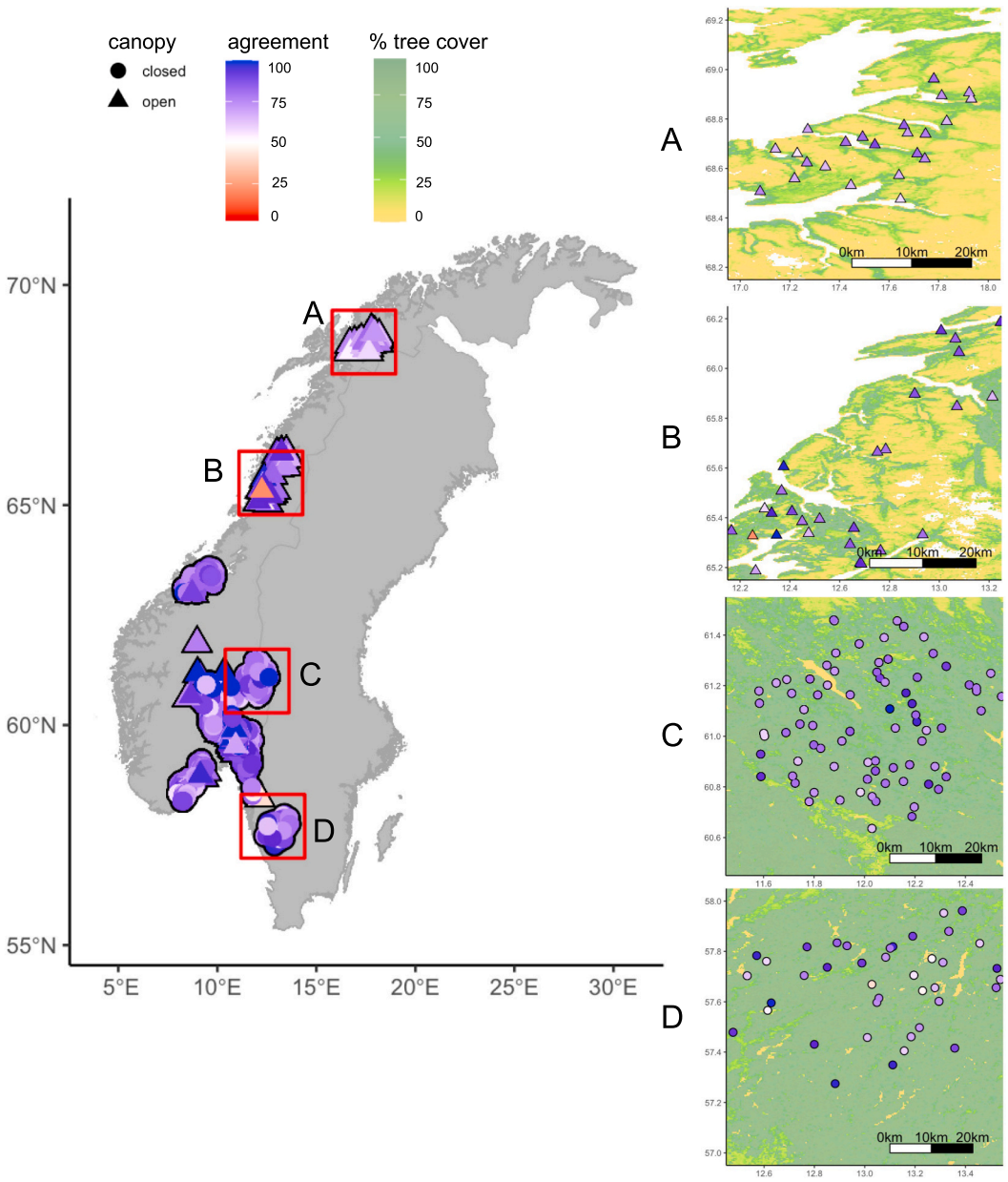

Fig. 5. Average agreement between snow cover from labeled images and MOD10A1 snow cover at Scandcam cameras between winter months for 2018–2020. The four boxes correspond to four example clusters in counties from north to south: A) north Nordland and Troms og Finnmark; B) south Nordland; C) Innlandet; and D) south Viken. The base map is tree canopy cover from 30-m Landsat. Triangles represent cameras within closed canopy areas (≥20%) and circles represent cameras within open canopy areas (< 20%). (For interpretation of the references to color in this figure legend, the reader is referred to the web version of this article).

3.3. Image labels and MOD10A1F product comparison

Cloud persistence was a significant predictor for agreement between image labels and snow values from the MOD10A1F product. Agreement was highest (78.5%) on clear sky days (i.e. cloud persistence = 0) and decreased by almost one third (to 56.4%) within the first 3 days before leveling off just after (Fig. 6).

3.4. Optimal threshold derivation for binary snow cover mapping

At the Youden's Index point of the ROC curve, the true positive rate was 88% and the false positive rate was 11%. This point corresponded to a MOD10A1 NDSI snow cover value of 40.5 (Fig. 7). At the commonly used threshold value of 40 (Hall et al., 2019a), the true positive rate was 89% and the false positive rate was 11%, showing that for a slightly higher true positive rate, there is not much difference in the false positive rate. The current MOD10A2 product employs a threshold of 10, which has a 97% true positive rate and 31% false negative rate. When we conducted separate analyses for closed canopy (≥ 20%) and open canopy (< 20%) sites, the threshold was the same for closed canopy locations (40.5) and slightly higher for open canopy locations (41.5). Appendix A8 shows the change in true positive and false positive rates with different threshold values, along with the results for open and closed canopy analyses.

4. Discussion

In this study, we identified strong agreement between snow information obtained from wildlife cameras and MODIS at a regional scale, demonstrating the ability of cameras to supplement MODIS snow observations. Previous studies have found strong agreement using fewer than 100 cameras in tandem with satellites at localized spatial scales

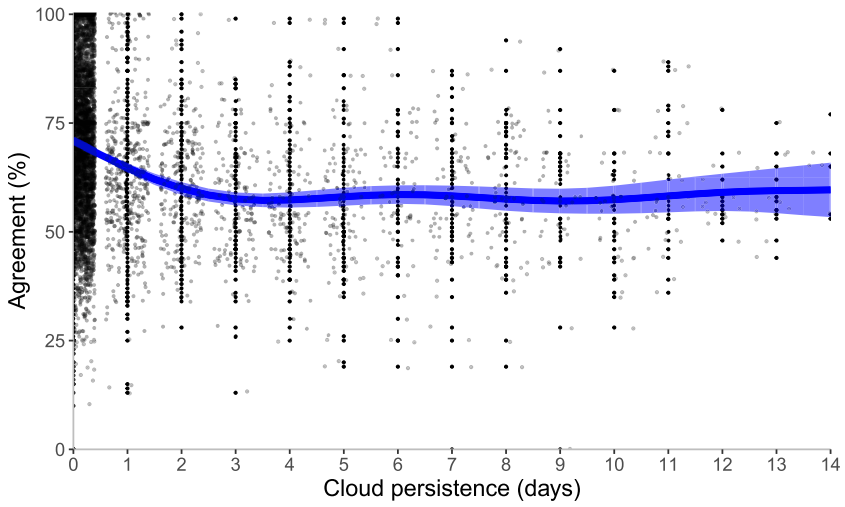

Fig. 6. Agreement between image labels and MOD10A1F NDSI snow values as a function of number of cloudy days (i.e., cloud persistence) using a generalized additive model. Agreement was defined as 100 minus the absolute difference between the image label and MOD10A1F NDSI snow value.

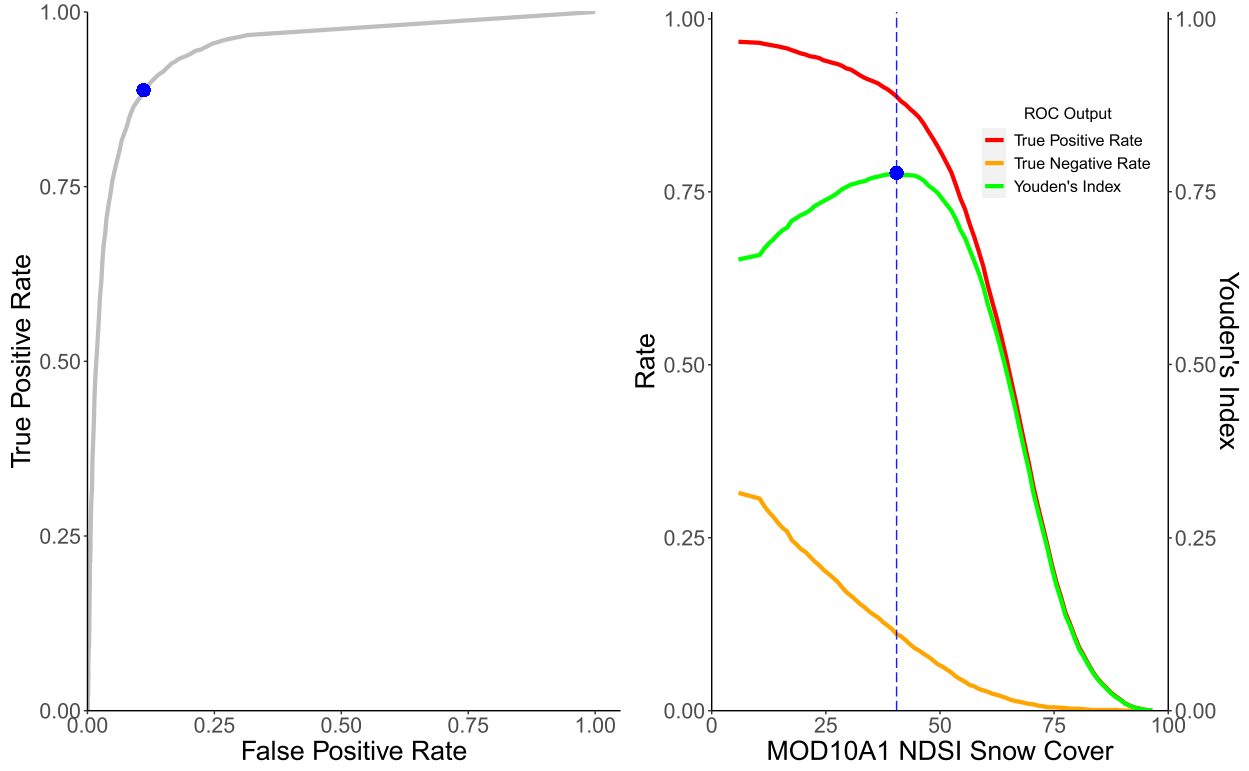

Fig. 7. A) A Receiver-Operator Characteristic (ROC) curve when images are reclassified for snow or no-snow by cutting the data with a label ≥ 1 as 'snow.' The ROC curve shows the performance of the classifier at each threshold, in this case the value of the NDSI snow cover. The closer the curve is to the top left corner, the better the performance of the model. The blue point closest to the top left corner is (0.11, 0.88) is referred to as Youden's Index. B) The true negative rate (orange) and the true positive rate (red) graphed separately for every MOD10A1 NDSI snow cover value alongside the Youden's Index, the difference in between (green). The MOD10A1 value at the maximum value of the Youden index is 40.50. The maximum value of the Youden index is the minimum between the true positive rate and true negative rate when both classes are given equal weight. The blue points on both graphs represent the same cut point in the data. (For interpretation of the references to color in this figure legend, the reader is referred to the web version of this article.)

(Raleigh et al., 2013; Sugiura et al., 2013), and our findings show this relationship holds across a large region and multiple winter seasons. As predicted, we found strongest agreement at low snow cover values, but agreement was worse than expected at high snow cover values because NDSI values plateaued around 75 instead of 100. Cameras, thus, demonstrated that an NDSI value of 75 represents 100% snow cover for this region. We also demonstrated the ability to customize MOD10A1 to create binary snow maps using a camera-derived threshold of 40.5, which was nearly identical to the commonly used 40 threshold from previous MODIS products (Klein et al., 1998). These findings highlight that despite large differences in scales, wildlife camera networks have potential to improve satellite monitoring for snow and create new products at fine temporal scales.

Our finding of strong agreement between camera image snow values and MODIS snow values may be attributed in part to our method of classifying snow cover into five classes. While not a continuous measure,

a 5-class ordinal labeling scheme for images extracts more information about the amount of snow cover than previous work using binary labels (Berman et al., 2018; Sugiura et al., 2013). There are caveats to this classification scheme, as agreement was lower at labels 1 (i.e., ~25% snow cover), 2 (i.e., ~50%), and 4 (i.e., ~100%), which may highlight MODIS uncertainties. For example, MODIS is less accurate when snow is thin or patchy, such as labels 1 and 2 (Berman et al., 2018; Dong and Menzel, 2016). Similarly, low agreement at label 4 highlights the tendency of MODIS to underestimate snow cover in boreal regions (Klein et al., 1998). In this region, maximum NDSI equating to 100% snow cover appears to be 75, when MODIS plateaus. Cameras can thus be used to adjust NDSI for fractional snow-covered maps. However, discrepancies in agreement at different classification schemes highlights drawbacks to using cameras in tandem with satellite products: patchy snow in cameras may be missed or interpreted as complete snow cover. Furthermore, labeling for snow cover values can be subjective and have uncertainty, as highlighted by low correspondence among labels by two observers found during pilot testing. We recommend a single, experienced labeler when labeling wildlife photos, and testing for agreement among labelers early on. Despite lower agreement within certain classes and among observers, strong agreement overall suggests that cameras can be an effective method of snow classification when used in tandem with satellites.

We predicted that latitude (i.e., solar zenith angles), ground vegetation, and the image color mode (i.e., grey or color scale) would limit MODIS and camera image agreement (Xiao et al., 2022; Xin et al., 2012). Although mapping the agreement at each of our cameras showed a general decline in agreement as latitude increased, the effect was not significant, and there was still strong agreement even at high latitudes. Overall, our findings indicated that latitude and canopy cover had relatively minor effects on the accuracy of MODIS snow cover, highlighting its robustness for monitoring snow trends across Scandinavia. Images in grey-scale had lower overall agreement with satellites, and they took much longer to label due to the need to study the image more carefully to separate snow from vegetation and rocks. Humans and artificial intelligence have more difficulty extracting information about environmental conditions and wildlife from grey-scale images (Beery et al., 2019; Favorskaya and Buryachenko, 2019). Nighttime images are inevitable when using motion-triggered wildlife cameras for environmental monitoring, but we recommend maximizing the number of color images either through prioritizing color photos as we did here, or by scheduling timelapse photos to occur during daylight hours. Because low-light images were also the main reason why images from one labeler had to be relabeled, prioritizing color photos may increase both agreement between camera and satellite as well as agreement among labelers.

Using cameras to assess agreement demonstrated drawbacks of using NDVI alongside MODIS NDSI. Contrary to our hypothesis, NDVI positively affected the agreement. While daily NDVI is often included to account for the effects of vegetation on MODIS snow detection (Hall et al., 2002; Klein et al., 1998; Xin et al., 2012), NDVI has multiple interpretations, including green-up, biomass, and plant stress (Huang et al., 2021). The positive effect of NDVI on snow cover agreement suggests that daily NDVI during winter may not have represented vegetation that was obscuring the sensor, but rather the absence of snow. We included snow values ranging from 0 to 100, but values equal to 0 for both camera images and MODIS will have exact agreement whereas our estimates for the other snow labels were approximations. When we excluded images from the month October, the month that also has the highest average NDVI at the camera locations, we found the expected negative relationship between NDVI and agreement for months between November and March. October data was important to include in our study because the "snow-on" date typically occurs during October in Norway, and this date is critical for deriving snow cover phenology metrics used by wildlife ecologists studying migration timing and other seasonal phenomena. However, the strong effect of October on the NDVI estimate reinforces that NDVI was reflecting the absence of snow rather than canopy cover. We also examined maximum NDVI over each snow-covered season as a covariate instead of daily NDVI, and we found similar results (Appendix A7). In contrast, the tree canopy cover covariate had a negative effect on agreement as expected, even with October data included. The Landsat tree canopy cover product is a more direct measure of obstructing vegetation than NDVI (Potapov et al., 2021; Sexton et al., 2013), and our findings indicate that direct canopy products may be preferable to NDVI for snow mapping applications.

Agreement was also affected by cloudy days, supporting previous literature on limitations of cloud-gap filled products in cloudy regions (Gao et al., 2011; Hall et al., 2019b). However, agreement did not decrease linearly with time, but instead decreased rapidly and then leveled off after 3 days. This result is likely due to clouds changing the snow conditions, such as snowstorms increasing snow cover or increased humidity accelerating snowmelt (Zhang et al., 1996). Backfilling pixels with the most recent cloud-free value thus has limitations even for short cloud persistence durations. In cases when clouds persist for much of the winter, our results show that gap-filled products may be highly inaccurate, and wildlife camera data in these regions is especially valuable. While cloud-masked MOD10A1 values had substantially higher agreement with camera images than gap-filled MOD10A1F values, use of the MOD10A1 product comes at the cost of substantial data loss, as only 23% of pixels were usable due to cloud masking. Similarly, a study examining how snow properties affect movements of GPS-collared Dall sheep (*Ovis dalli dalli*) in Lake Clark National Park, Alaska, was only able to use 2.2% of their dataset when using cloud-masked MODIS products (Mahoney et al., 2018). Ultimately, spatial products of snow cover may be able to automate the inclusion of snow values from camera networks when satellite values are not accurate or available, utilizing AI and machine learning to produce spatially and temporally fill gaps.

Gap-filling accuracy with camera-labeled values will depend on classification accuracy, and image classification error may be further reduced by using a binary classification, although some information is lost. However, binary maps can be especially useful for identifying snow-on and snow-off dates, with important applications for monitoring changing snow phenology and impacts on seasonal migrations and breeding seasons. The threshold NDSI value of 40.5 we identified using wildlife cameras in Scandinavia was remarkably similar to the value of 40 derived for MODIS from Landsat fractional snow-covered area maps in Canada (Klein et al., 1998). Thresholds in forested areas tend to be lower than open canopy thresholds because some snow visibility is blocked by the trees (Chokmani et al., 2010). Our findings were consistent with these trends, but the effect of canopy cover was minor (40.5 vs 41.5 for closed vs open canopy sites, respectively). By employing Youden's index to select the optimal threshold, we assumed equal weight to both snow and no snow classes. However, depending on the mapping needs, other threshold values could be used. For example, higher thresholds for snow might be desirable when making maps of the first "snow on" date in the fall to prioritize snow detection. Other studies have found adjustments to the threshold can increase regional accuracy (Chokmani et al., 2010; Da Ronco et al., 2020; Luo et al., 2022). While our study found that MODIS detected 88% of snow-covered pixels, Luo et al. (2022) found that MODIS identified just 14–18% of snow-covered pixels in forests when using conventional MODIS thresholds. MODIS snow detection tends to be less accurate in steep areas with complex topography (Rittger et al., 2021), and the Luo et al. (2022) study occurred in alpine terrain with sites >2700 m a.s.l. and slopes between 19 and 34°. Our study occurred at much lower elevations (0–800 m a.s.l.), with moderate slopes between 0.5 and 20°. These differences reinforce our findings that agreement between camera and satellite may depend on environmental factors, and when using the two for validation or in-tandem, it is important to account for external context. Generally, a threshold of 40 is robust for this region, similar to other studies creating binary maps from forested ecosystems. A threshold of 10 from MOD10A2 would be low for this region, thus researchers should be aware that deriving their own binary thresholds is an important step for

MODIS Collection 6 products. Future studies could employ this approach to create custom thresholds from cameras in their regions of interest.

Because our cameras were optimized for lynx detection, we did not control for field of view. Previous work suggests that wider field of views are more advantageous for snow cover monitoring (Parajka et al., 2012). Our results suggest that even narrow fields of view offer insight into snow conditions, but wider fields should provide a better observation of snow conditions at a scale more similar to satellite remote sensing. Additionally, we did not control for possible observation delays, which could be up to 24 h depending on when the satellite passes over the area of interest and when the camera image is taken (Sugiura et al., 2013). One camera trap image per day appeared sufficient to connect to MODIS, but we recommend multiple images per camera each day to increase labeling options. Examining the outliers from our model evaluations aligns with these recommendations, because outlier images consisted primarily of those with narrow fields of view and active weather (Appendix A9). Continuous indices of vegetation greenness have been derived from camera images using RGB values as proxies for vegetation (Sun et al., 2021), but to our knowledge, no automated method of extracting continuous snow cover indices from camera images has been developed. AI algorithms for automated snow detection from camera images are a promising area of development to increase the utility of wildlife camera networks for environmental monitoring.

Our study focused on comparing snow cover from cameras to MODIS snow products, and we found surprisingly strong agreement considering differences in spatial resolution. The Visible Infrared Imaging Radiometer Suite (VIIRS) instrument has a snow product similar to MODIS at 375-m spatial resolution (Riggs et al., 2017). Future work could explore incorporating multiple cameras in one satellite pixel to improve snow monitoring of patchy snow conditions, such as during snow accumulation and snow melt. Alternatively, camera images could be matched to finer-resolution snow products derived from satellites such as Landsat, Sentinel, and Planet CubeSat (Cannistra et al., 2021; Chokmani et al., 2010; Riggs et al., 2017). Snow maps must be derived by manually creating the NDSI maps from Landsat, Sentinel, and Planet sensors, but these products have spatial resolutions at 30 m, 10 m, and 0.7–3 m, respectively, closer to the camera field of view (Cannistra et al., 2021).

5. Conclusion

As the remote sensing community continues to develop new global products, the wildlife ecology community continues to expand camera trap networks for continuous biodiversity monitoring (Pettorelli et al., 2014; Steenweg et al., 2017). Connecting camera traps to satellite data represents an important step towards an interconnected network of ground-based remote sensing data that can improve researchers' and the public's ability to determine environmental changes and subsequent impacts on sensitive species. In Norway, snow cover extent has decreased by >20,000 km^2 (6% of the country area) since 1961 due to changes in temperature and precipitation (Rizzi et al., 2018; Skaugen et al., 2012). When these trends are incorporated into climate impact models, predictions suggest accelerated rates of local extinctions across 273 species of Norwegian vegetation (Niittynen et al., 2018). With the increasing number of cameras operating as environmental monitoring devices, we can improve our understanding of both environmental and wildlife responses in a changing climate.

Description of author's responsibilities

LRP and CB conceived of the idea. CB labeled images, ran statistical analyses, and led the writing. JO managed camera data and provided data access. DH and CV provided remote sensing expertise. All authors edited the manuscript.

Funding

This research was supported by the Erasmus Mobility + Exchange as well as NASA Graduate Fellowship Program Grant # 80NSSC19K1673. The Scandcam project was supported by the Norwegian Environment Agency, the Research Council of Norway (grants 251112 and 281092).

CRediT authorship contribution statement

Catherine Breen: Methodology, Writing – original draft, Formal analysis, Visualization, Investigation, Funding acquisition. **Carrie Vuyovich:** Supervision, Funding acquisition, Writing – review & editing. **John Odden:** Resources, Funding acquisition, Writing – review & editing. **Dorothy Hall:** Writing – review & editing. **Laura Prugh:** Writing – review & editing, Conceptualization, Supervision, Funding acquisition, Investigation.

Declaration of Competing Interest

The authors declare that they have no known competing financial interests or personal relationships that could have appeared to influence the work reported in this paper.

Data availability

A selection of photos is publicly available at https://viltkamera.nina.no. Analysis code can be found at https://github.com/catherine-m-breen/MODIS-Snow-Cover-to-Binary-Snow-Covered-Area. GEE assets are available at the following links: https://code.earthengine.google.com/?asset=users/catherinembreen/MODIS_Norway

Acknowledgements

We thank Sunniva Bahlk, Nina Myhr, Solveig Haug, for help in obtaining Scandcam images. Calum Cunningham and Michael Procko provided useful comments on preliminary drafts and analytical considerations, and members of the Prugh Lab provided valuable feedback on manuscript drafts.

Appendix A. Supplementary data

Supplementary data to this article can be found online at https://doi.org/10.1016/j.rse.2023.113648.

References

Beery, S., Wu, G., Rathod, V., Votel, R., Huang, J., 2019. Long Term Temporal Context for Per-Camera Object Detection. ArXiv191203538 Cs Eess Q-Bio.

Berman, E.E., Bolton, D.K., Coops, N.C., Mityok, Z.K., Stenhouse, G.B., Moore, R.D. (Dan), 2018. Daily estimates of Landsat fractional snow cover driven by MODIS and dynamic time-warping. Remote Sens. Environ. 216, 635–646. https://doi.org/10.1016/j.rse.2018.07.029.

Bivand, R., 2022. R packages for analyzing spatial data: a comparative case study with areal data. Geogr. Anal. 54, 488–518. https://doi.org/10.1111/gean.12319.

Boelman, N.T., Liston, G.E., Gurarie, E., Meddens, A.J.H., Mahoney, P.J., Kirchner, P.B., Bohrer, G., Brinkman, T.J., Cosgrove, C.L., Eitel, J.U.H., Hebblewhite, M., Kimball, J. S., LaPoint, S., Nolin, A.W., Pedersen, S.H., Prugh, L.R., Reinking, A.K., Vierling, L. A., 2019. Integrating snow science and wildlife ecology in Arctic-boreal North America. Environ. Res. Lett. 14, 010401 https://doi.org/10.1088/1748-9326/aaeec1.

Bokhorst, S., 2016. Changing Arctic snow cover: A review of recent developments and assessment of future needs for observations, modelling, and impacts, p. 22.

Bouyer, Y., San Martin, G., Poncin, P., Beudels-Jamar, R.C., Odden, J., Linnell, J.D.C., 2015. Eurasian lynx habitat selection in human-modified landscape in Norway: effects of different human habitat modifications and behavioral states. Biol. Conserv. 191, 291–299. https://doi.org/10.1016/j.biocon.2015.07.007.

Brooks, M.E., Kristensen, K., van Benthem, K.J., Magnusson, A., Berg, C.W., Nielsen, A., Skaug, H.J., Mächler, M., Bolker, B.M., 2017. glmmTMB balances speed and flexibility among packages for zero-inflated generalized linear mixed modeling. R Journal 9, 378. https://doi.org/10.32614/RJ-2017-066.

Brown, R.D., Mote, P.W., 2009. The response of northern hemisphere snow cover to a changing climate. J. Clim. 22, 2124–2145. https://doi.org/10.1175/2008JCLI2665.1.

Brown, T.B., Hultine, K.R., Steltzer, H., Denny, E.G., Denslow, M.W., Granados, J., Henderson, S., Moore, D., Nagai, S., SanClements, M., Sánchez-Azofeifa, A., Sonnentag, O., Tazik, D., Richardson, A.D., 2016. Using phenocams to monitor our changing Earth: toward a global phenocam network. Front. Ecol. Environ. 14, 84–93. https://doi.org/10.1002/fee.1222.

Cannistra, A.F., Shean, D.E., Cristea, N.C., 2021. High-resolution CubeSat imagery and machine learning for detailed snow-covered area. Remote Sens. Environ. 258, 112399 https://doi.org/10.1016/j.rse.2021.112399.

Carricondo-Sanchez, D., Odden, M., Linnell, J.D.C., Odden, J., 2017. The range of the mange: spatiotemporal patterns of sarcoptic mange in red foxes (Vulpes vulpes) as revealed by camera trapping. PLoS One 12, e0176200. https://doi.org/10.1371/journal.pone.0176200.

Chokmani, K., Dever, K., Bernier, M., Gauthier, Y., Paquet, L.-M., 2010. Adaptation of the SNOWMAP algorithm for snow mapping over eastern Canada using Landsat-TM imagery. Hydrol. Sci. J. 55, 649–660. https://doi.org/10.1080/02626661003747374.

Coll, J., Li, X., 2018. Comprehensive accuracy assessment of MODIS daily snow cover products and gap filling methods. ISPRS J. Photogramm. Remote Sens. 144, 435–452. https://doi.org/10.1016/j.isprsjprs.2018.08.004.

Crawford, C.J., 2015. MODIS Terra collection 6 fractional snow cover validation in mountainous terrain during spring snowmelt using Landsat TM and ETM+. Hydrol. Process. 29, 128–138. https://doi.org/10.1002/hyp.10134.

Curk, T., Pokrovsky, I., Lecomte, N., Aarvak, T., Brinker, D.F., Burnham, K., Dietz, A., Dixon, A., Franke, A., Gauthier, G., Jacobsen, K.-O., Kidd, J., Lewis, S.B., Øien, I.J., Sokolov, A., Sokolov, V., Solheim, R., Weidensaul, S., Wiebe, K., Wikelski, M., Therrien, J.-F., Safi, K., 2020. Arctic avian predators synchronise their spring migration with the northern progression of snowmelt. Sci. Rep. 10, 7220. https://doi.org/10.1038/s41598-020-63312-0.

Da Ronco, P., Avanzi, F., De Michele, C., Notarnicola, C., Schaefli, B., 2020. Comparing MODIS snow products Collection 5 with Collection 6 over Italian Central Apennines. Int. J. Remote Sens. 41, 4174–4205. https://doi.org/10.1080/01431161.2020.1714778.

Didan, K., 2015. MOD13A1 MODIS/Terra Vegetation Indices 16-Day L3 Global 500m SIN Grid V006. NASA LP DAAC. https://doi.org/10.5067/MODIS/MOD13A1.006.

Dong, C., Menzel, L., 2016. Producing cloud-free MODIS snow cover products with conditional probability interpolation and meteorological data. Remote Sens. Environ. 186, 439–451. https://doi.org/10.1016/j.rse.2016.09.019.

Dormann, C.F., Elith, J., Bacher, S., Buchmann, C., Carl, G., Carré, G., Marquéz, J.R.G., Gruber, B., Lafourcade, B., Leitão, P.J., Münkemüller, T., McClean, C., Osborne, P.E., Reineking, B., Schröder, B., Skidmore, A.K., Zurell, D., Lautenbach, S., 2013. Collinearity: a review of methods to deal with it and a simulation study evaluating their performance. Ecography 36, 27–46. https://doi.org/10.1111/j.1600-0587.2012.07348.x.

Favorskaya, M., Buryachenko, V., 2019. Selecting informative samples for animal recognition in the wildlife. In: Czarnowski, I., Howlett, R.J., Jain, L.C. (Eds.), Intelligent Decision Technologies 2019, Smart Innovation, Systems and Technologies. Springer Singapore, Singapore, pp. 65–75. https://doi.org/10.1007/978-981-13-8303-8_6.

Forrester, T., O'Brien, T., Fegraus, E., Jansen, P., Palmer, J., Kays, R., Ahumada, J., Stern, B., McShea, W., 2016. An open standard for camera trap data. Biodivers. Data J. 4, e10197 https://doi.org/10.3897/BDJ.4.e10197.

Franklin, S.E., 2020. Interpretation and use of geomorphometry in remote sensing: a guide and review of integrated applications. Int. J. Remote Sens. 41, 7700–7733. https://doi.org/10.1080/01431161.2020.1792577.

Gao, Y., Lu, N., Yao, T., 2011. Evaluation of a cloud-gap-filled MODIS daily snow cover product over the Pacific Northwest USA. J. Hydrol. 404, 157–165. https://doi.org/10.1016/j.jhydrol.2011.04.026.

Garvelmann, J., Pohl, S., Weiler, M., 2013. From observation to the quantification of snow processes with a time-lapse camera network. Hydrol. Earth Syst. Sci. 17, 1415–1429. https://doi.org/10.5194/hess-17-1415-2013.

Hall, D.K., Riggs, G.A., 2007. Accuracy assessment of the MODIS snow products. Hydrol. Process. 21, 1534–1547. https://doi.org/10.1002/hyp.6715.

Hall, D.K., Kelly, R.E.J., Riggs, G.A., Chang, A.T.C., Foster, J.L., 2002. Assessment of the relative accuracy of hemispheric-scale snow-cover maps. Ann. Glaciol. 34, 24–30. https://doi.org/10.3189/172756402781817770.

Hall, D.K., Riggs, G.A., Foster, J.L., Kumar, S.V., 2010. Development and evaluation of a cloud-gap-filled MODIS daily snow-cover product. Remote Sens. Environ. 114, 496–503. https://doi.org/10.1016/j.rse.2009.10.007.

Hall, D.K., Riggs, G.A., Solomonson, V., 2016. MODIS/Terra Snow Cover Daily L3 Global 500m SIN Grid, Version 6. NASA National Snow and Ice Data Center Distributed Active Archive Center, Boulder, Colorado USA. https://doi.org/10.5067/MODIS/MOD10A1.006.

Hall, D.K., Riggs, G.A., DiGirolamo, N.E., Román, M.O., 2019a. MODIS Cloud-Gap Filled Snow-Cover Products: Advantages and Uncertainties (preprint). Snow and Ice/Remote Sensing and GIS. https://doi.org/10.5194/hess-2019-123.

Hall, D.K., Riggs, G.A., DiGirolamo, N.E., Román, M.O., 2019b. Evaluation of MODIS and VIIRS cloud-gap-filled snow-cover products for production of an earth science data record. Hydrol. Earth Syst. Sci. 23, 5227–5241. https://doi.org/10.5194/hess-23-5227-2019.

Hao, X., Huang, G., Zheng, Z., Sun, X., Ji, W., Zhao, H., Wang, J., Li, H., Wang, X., 2022. Development and validation of a new MODIS snow-cover-extent product over China. Hydrol. Earth Syst. Sci. 26, 1937–1952. https://doi.org/10.5194/hess-26-1937-2022.

Hartig, F., 2022. DHARMa: Residual Diagnostics for Hierarchical (Multi-Level / Mixed) Regression Models. R package version 0.4.6. https://CRAN.R-project.org/package=DHARMa.

Hofmeester, T.R., Young, S., Juthberg, S., Singh, N.J., Widemo, F., Andrén, H., Linnell, J. D.C., Cromsigt, J.P.G.M., 2019. Using by-catch data from wildlife surveys to quantify climatic parameters and the timing of phenology for plants and animals using camera traps. Remote Sens. Ecol. Conserv. rse2.136 https://doi.org/10.1002/rse2.136.

Huang, X., Liang, T., Zhang, X., Guo, Z., 2011. Validation of MODIS snow cover products using Landsat and ground measurements during the 2001–2005 snow seasons over northern Xinjiang, China. Int. J. Remote Sens. 32, 133–152. https://doi.org/10.1080/01431160903439924.

Huang, S., Tang, L., Hupy, J.P., Wang, Y., Shao, G., 2021. A commentary review on the use of normalized difference vegetation index (NDVI) in the era of popular remote sensing. J. For. Res. 32, 1–6. https://doi.org/10.1007/s11676-020-01155-1.

Klein, A.G., Hall, D.K., Riggs, G.A., 1998. Improving snow cover mapping in forests through the use of a canopy reflectance model. Hydrol. Process. 12, 1723–1744. https://doi.org/10.1002/(SICI)1099-1085(199808/09)12:10/11<1723::AID-HYP691>3.0.CO;2-2.

Laforge, M.P., Bonar, M., Vander Wal, E., 2021. Tracking snowmelt to jump the green wave: phenological drivers of migration in a northern ungulate. Ecology 102. https://doi.org/10.1002/ecy.3268.

Liang, T., Huang, X., Wu, C., Liu, X., Li, W., Guo, Z., Ren, J., 2008. An application of MODIS data to snow cover monitoring in a pastoral area: a case study in Northern Xinjiang, China. Remote Sens. Environ. 112, 1514–1526. https://doi.org/10.1016/j.rse.2007.06.001.

Liu, X., 2012. Classification accuracy and cut point selection. Stat. Med. 31, 2676–2686. https://doi.org/10.1002/sim.4509.

Luo, J., Dong, C., Lin, K., Chen, X., Zhao, L., Menzel, L., 2022. Mapping snow cover in forests using optical remote sensing, machine learning and time-lapse photography. Remote Sens. Environ. 275, 113017 https://doi.org/10.1016/j.rse.2022.113017.

Lussana, C., Saloranta, T., Skaugen, T., Magnusson, J., Tveito, O.E., Andersen, J., 2018. seNorge2 daily precipitation, an observational gridded dataset over Norway from 1957 to the present day. Earth Syst. Sci. Data 10, 235–249. https://doi.org/10.5194/essd-10-235-2018.

Madsen, J., Tamstorf, M., Klaassen, M., Eide, N., Glahder, C., Rigét, F., Nyegaard, H., Cottaar, F., 2007. Effects of snow cover on the timing and success of reproduction in high-Arctic pink-footed geese *Anser brachyrhynchus*. Polar Biol. 30, 1363–1372. https://doi.org/10.1007/s00300-007-0296-9.

Mahoney, P.J., Liston, G.E., LaPoint, S., Gurarie, E., Mangipane, B., Wells, A.G., Brinkman, T.J., Eitel, J.U.H., Hebblewhite, M., Nolin, A.W., Boelman, N., Prugh, L. R., 2018. Navigating snowscapes: scale-dependent responses of mountain sheep to snowpack properties. Ecol. Appl. 28, 1715–1729. https://doi.org/10.1002/eap.1773.

Mankin, J.S., Viviroli, D., Singh, D., Hoekstra, A.Y., Diffenbaugh, N.S., 2015. The potential for snow to supply human water demand in the present and future. Environ. Res. Lett. 10, 114016 https://doi.org/10.1088/1748-9326/10/11/114016.

McHugh, M.L., 2012. Interrater reliability: the kappa statistic. Biochem. Med. 276–282 https://doi.org/10.11613/BM.2012.031.

Negi, H.S., Thakur, N.K., Mishra, V.D., 2007. Estimation and validation of snow surface temperature using modis data for snow-avalanche studies in NW-Himalaya. J. Indian Soc. Remote Sens. 35, 287–299. https://doi.org/10.1007/BF02990785.

Niittynen, P., Heikkinen, R.K., Luoto, M., 2018. Snow cover is a neglected driver of Arctic biodiversity loss. Nat. Clim. Chang. 8, 997–1001. https://doi.org/10.1038/s41558-018-0311-x.

Nolin, A.W., 2010. Recent advances in remote sensing of seasonal snow. J. Glaciol. 56, 1141–1150. https://doi.org/10.3189/002214311796406077.

Parajka, J., Haas, P., Kirnbauer, R., Jansa, J., Blöschl, G., 2012. Potential of time-lapse photography of snow for hydrological purposes at the small catchment scale: POTENTIAL OF TIME-LAPSE PHOTOGRAPHY OF SNOW FOR HYDROLOGICAL PURPOSES. Hydrol. Process. 26, 3327–3337. https://doi.org/10.1002/hyp.8389.

Pettorelli, N., Laurance, W.F., O'Brien, T.G., Wegmann, M., Nagendra, H., Turner, W., 2014. Satellite remote sensing for applied ecologists: opportunities and challenges. J. Appl. Ecol. 51, 839–848. https://doi.org/10.1111/1365-2664.12261.

Potapov, P., Li, X., Hernandez-Serna, A., Tyukavina, A., Hansen, M.C., Kommareddy, A., Pickens, A., Turubanova, S., Tang, H., Silva, C.E., Armston, J., Dubayah, R., Blair, J. B., Hofton, M., 2021. Mapping global forest canopy height through integration of GEDI and Landsat data. Remote Sens. Environ. 253, 112165 https://doi.org/10.1016/j.rse.2020.112165.

Raleigh, M.S., Rittger, K., Moore, C.E., Henn, B., Lutz, J.A., Lundquist, J.D., 2013. Ground-based testing of MODIS fractional snow cover in subalpine meadows and forests of the Sierra Nevada. Remote Sens. Environ. 128, 44–57. https://doi.org/10.1016/j.rse.2012.09.016.

Reinking, A.K., Højlund Pedersen, S., Elder, K., Boelman, N.T., Glass, T.W., Oates, B.A., Bergen, S., Roberts, S., Prugh, L.R., Brinkman, T.J., Coughenour, M.B., Feltner, J.A., Barker, K.J., Bentzen, T.W., Pedersen, Å.Ø., Schmidt, N.M., Liston, G.E., 2022. Collaborative wildlife–snow science: integrating wildlife and snow expertise to improve research and management. Ecosphere 13. https://doi.org/10.1002/ecs2.4094.

Riggs, G.A., Hall, D.K., Román, M.O., 2017. Overview of NASA's MODIS and visible infrared imaging radiometer suite (VIIRS) snow-cover Earth system data records. Earth Syst. Sci. Data 9, 765–777. https://doi.org/10.5194/essd-9-765-2017.

Riggs, G.A., Hall, D.K., Román, M.O., 2019. MODIS Snow Products Collection 6.1 User Guide, Version 1.0. NASA Goddard Space Flight Center. https://modis-snow-ice-gsfc.nasa.gov/?c=userguides.

Rittger, K., Bormann, K.J., Bair, E.H., Dozier, J., Painter, T.H., 2021. Evaluation of VIIRS and MODIS snow cover fraction in High-Mountain Asia using Landsat 8 OLI. Front. Remote Sens. 2, 647154 https://doi.org/10.3389/frsen.2021.647154.

Rizzi, J., Nilsen, I.B., Stagge, J.H., Gisnås, K., Tallaksen, L.M., 2018. Five decades of warming: impacts on snow cover in Norway. Hydrol. Res. 49, 670–688. https://doi.org/10.2166/nh.2017.051.

Robin, X., Turck, N., Hainard, A., Tiberti, N., Lisacek, F., Sanchez, J.-C., Müller, M., 2011. pROC: an open-source package for R and S+ to analyze and compare ROC curves. BMC Bioinform. 12, 77. https://doi.org/10.1186/1471-2105-12-77.

Saloranta, T.M., 2012. Simulating snow maps for Norway: description and statistical evaluation of the seNorge snow model. Cryosphere 6, 1323–1337. https://doi.org/10.5194/tc-6-1323-2012.

Sexton, J.O., Song, X.-P., Feng, M., Noojipady, P., Anand, A., Huang, C., Kim, D.-H., Collins, K.M., Channan, S., DiMiceli, C., Townshend, J.R., 2013. Global, 30-m resolution continuous fields of tree cover: Landsat-based rescaling of MODIS vegetation continuous fields with lidar-based estimates of error. Int. J. Digit. Earth 6, 427–448. https://doi.org/10.1080/17538947.2013.786146.

Sirén, A.P.K., Somos-Valenzuela, M., Callahan, C., Kilborn, J.R., Duclos, T., Tragert, C., Morelli, T.L., 2018. Looking beyond wildlife: using remote cameras to evaluate accuracy of gridded snow data. Remote Sens. Ecol. Conserv. 4, 375–386. https://doi.org/10.1002/rse2.85.

Skaugen, T., Stranden, H.B., Saloranta, T., 2012. Trends in snow water equivalent in Norway (1931–2009). Hydrol. Res. 43, 489–499. https://doi.org/10.2166/nh.2012.109.

Solomon, S., Qin, D., Manning, M., Marquis, M., Averyt, K., Tignor, M., LeRoy Miller, H., Chen, Z., 2007. Climate Change 2007: The Physical Science Basis: Contribution of Working Group I to the Fourth Assessment Report of the Intergovernmental Panel on Climate Change. Cambridge University Press, Cambridge, New York.

Sonnentag, O., Hufkens, K., Teshera-Sterne, C., Young, A.M., Friedl, M., Braswell, B.H., Milliman, T., O'Keefe, J., Richardson, A.D., 2012. Digital repeat photography for phenological research in forest ecosystems. Agric. For. Meteorol. 152, 159–177. https://doi.org/10.1016/j.agrformet.2011.09.009.

Steenweg, R., Hebblewhite, M., Kays, R., Ahumada, J., Fisher, J.T., Burton, C., Townsend, S.E., Carbone, C., Rowcliffe, J.M., Whittington, J., Brodie, J., Royle, J.A., Switalski, A., Clevenger, A.P., Heim, N., Rich, L.N., 2017. Scaling-up camera traps: monitoring the planet's biodiversity with networks of remote sensors. Front. Ecol. Environ. 15, 26–34. https://doi.org/10.1002/fee.1448.

Sugiura, K., Nagai, S., Nakai, T., Suzuki, R., 2013. Application of time-lapse digital imagery for ground-truth verification of satellite indices in the boreal forests of Alaska. Polar Sci. 7, 149–161. https://doi.org/10.1016/j.polar.2013.02.003.

Sun, C., Beirne, C., Burgar, J.M., Howey, T., Fisher, J.T., Burton, A.C., 2021. Simultaneous monitoring of vegetation dynamics and wildlife activity with camera traps to assess habitat change. Remote Sens. Ecol. Conserv. 7, 666–684. https://doi.org/10.1002/rse2.222.

Thapa, S., Chhetri, P.K., Klein, A.G., 2019. Cross-comparison between MODIS and VIIRS snow cover products for the 2016 hydrological year. Climate 7, 57. https://doi.org/10.3390/cli7040057.

Tobler, M.W., Zúñiga Hartley, A., Carrillo-Percastegui, S.E., Powell, G.V.N., 2015. Spatiotemporal hierarchical modelling of species richness and occupancy using camera trap data. J. Appl. Ecol. 52, 413–421. https://doi.org/10.1111/1365-2664.12399.

Townshend, J., 2016. Global Forest Cover Change (GFCC) Forest Cover Change Multi-Year Global 30 m V001. NASA LP DAAC. https://doi.org/10.5067/MEASURES/GFCC/GFCC30FCC.001.

Urbanek, R.E., Ferreira, H.J., Olfenbuttel, C., Dukes, C.G., Albers, G., 2019. See what you've been missing: an assessment of Reconyx® PC900 Hyperfire cameras. Wildl. Soc. Bull. 43, 630–638. https://doi.org/10.1002/wsb.1015.

Wood, S.N., 2017. Generalized Additive Models: An Introduction with R, 2nd edition. Chapman and Hall/CRC. https://doi.org/10.1201/9781315370279.

Wuertz, D., Setz, T., Chalabi, Y., Boshnakov, G., 2023. timeDate: Rmetrics - Chronological and Calendar Objects. R package version, 4022, p. 108. https://CRAN.R-project.org/package=timeDate.

Xiao, X., He, T., Liang, Shunlin, Liu, X., Ma, Y., Liang, Shuang, Chen, X., 2022. Estimating fractional snow cover in vegetated environments using MODIS surface reflectance data. Int. J. Appl. Earth Obs. Geoinf. 114, 103030 https://doi.org/10.1016/j.jag.2022.103030.

Xin, Q., Woodcock, C.E., Liu, J., Tan, B., Melloh, R.A., Davis, R.E., 2012. View angle effects on MODIS snow mapping in forests. Remote Sens. Environ. 118, 50–59. https://doi.org/10.1016/j.rse.2011.10.029.

Youden, W.J., 1950. Index for rating diagnostic tests. Cancer 3, 32–35. https://doi.org/10.1002/1097-0142(1950)3:1<32::AID-CNCR2820030106>3.0.CO;2-3.

Zhang, T., Stamnes, K., Bowling, S.A., 1996. Impact of clouds on surface radiative fluxes and snowmelt in the Arctic and Subarctic. J. Clim. 9, 2110–2123. https://doi.org/10.1175/1520-0442(1996)009<2110:IOCOSR>2.0.CO;2.

Zhang, H., Zhang, F., Zhang, G., Che, T., Yan, W., Ye, M., Ma, N., 2019. Ground-based evaluation of MODIS snow cover product V6 across China: implications for the selection of NDSI threshold. Sci. Total Environ. 651, 2712–2726. https://doi.org/10.1016/j.scitotenv.2018.10.128.

Zuur, A.F., Ieno, E.N., Elphick, C.S., 2010. A protocol for data exploration to avoid common statistical problems: *Data exploration*. Methods Ecol. Evol. 1, 3–14. https://doi.org/10.1111/j.2041-210X.2009.00001.x.